ELSEVIER

Journal of Structural Geology 27 (2005) 2171–2180

JOURNAL OF STRUCTURAL GEOLOGY

www.elsevier.com/locate/jsg

2D rotation of rigid inclusions in confined bulk simple shear flow: a numerical study

Fernando O. Marques[a,*], Rui M. Taborda[b], José V. Antunes[c]

[a]Departmento de Geologia and CGUL, Faculdade de Ciências, Universidade de Lisboa, Edifício C6, Piso 2, 1749-016 Lisboa, Portugal
[b]Departmento de Geologia and LATTEX, Faculdade de Ciências, Universidade de Lisboa, Edificio C6, Piso 2, 1749-016 Lisboa Portugal
[c]Applied Dynamics Laboratory, Instituto Tecnológico e Nuclear, Estrada Nacional 10, 2686 Sacavém, Portugal

Received 6 February 2005; received in revised form 5 June 2005; accepted 12 August 2005
Available online 3 October 2005

Abstract

We have used incompressible Navier–Stokes in 2D finite element modelling to investigate rigid inclusion rotation under confined bulk simple shear flow. Confinement is defined as the ratio (S) between the channel width (H) and the inclusion's least axis (e_2)($S=H/e_2$). The numerical results show that (i) inclusion rotation is strongly influenced by S and, when the confinement is effective, aspect ratio (R) and shape also play an important role. (ii) Back rotation is limited because inclusions reach a stable equilibrium orientation (ϕ_{se}). (iii) There is also an unstable equilibrium orientation (ϕ_{ue}), which defines an antithetic rotation field with ϕ_{se}, and both ϕ_{se} and ϕ_{ue} depend on S, and inclusion R and shape.

Keywords: Numerical modelling; Inclusion rotation; Inclusion shape; Confined simple shear; Stable equilibrium orientations; SPO

1. Introduction

The study of ductile shear zones is crucial to an understanding of tectonic shortening at depth and exhumation of deep-seated rocks to shallow levels in the lithosphere. However, many of the mylonitic rocks now observed at the Earth's surface have undergone more or less severe late recrystallisation, which has erased most of the features necessary to understand the mechanics of mylonite generation and evolution. Therefore, much effort has been put into the physical and theoretical modelling of rock behaviour, and authors like Passchier et al. (1993), Hudleston and Lan (1994) and Schmalholz and Podladchikov (2001) have pointed out the importance of the use of geometrical patterns in deformed rocks to constrain rock rheology.

The study of natural mylonites has shown that Jeffery's theory (Jeffery, 1922) for rigid ellipsoid rotation in simple shear is not directly applicable in many natural cases, because many rigid inclusions show no signs of rotation and many fabrics seem to be stable (rotation rate equal to zero). This is one reason that there has been a concentration of research on the factors that could alter the rotation behaviour of rigid inclusions, such as: (i) the addition of a pure shear component (e.g. Ghosh and Ramberg, 1976; Passchier, 1987; Ježek et al., 1996; Marques and Coelho, 2003), (ii) inclusion interaction in multi-inclusion systems (e.g. Fernandez et al., 1983; Ildefonse et al., 1992a,b; Ježek et al., 1994; Samanta et al., 2003), (iii) slipping boundary between inclusion and matrix (e.g. Ildefonse and Mancktelow, 1993; Marques and Cobbold, 1995; Marques and Coelho, 2001; Arbaret et al., 2001; Pennacchioni et al., 2001; Mancktelow et al., 2002; Ceriani et al., 2003; Marques and Bose, 2004; Schmid and Podladchikov, 2004), and (iv) confined flow (e.g. Marques and Cobbold, 1995; Pennacchioni et al., 2000; Marques and Coelho, 2001; Biermeier et al., 2001; Taborda et al., 2004; Marques et al., 2005). Confinement is defined as the ratio (S) between shear zone width (H) and inclusion's least principal axis (e_2) ($S=H/e_2$). Experimental and theoretical work by Marques and Cobbold (1995), Marques and Coelho (2001), Taborda et al. (2004) and Marques et al. (2005) has shown that confinement can affect the matrix flow and, thus, the

* Corresponding author. Tel.: +351 217 500 000; fax: +351 217 500 064.
E-mail address: fmarques@fc.ul.pt (F.O. Marques).

0191-8141/$ - see front matter © 2005 Elsevier Ltd. All rights reserved.
doi:10.1016/j.jsg.2005.08.008

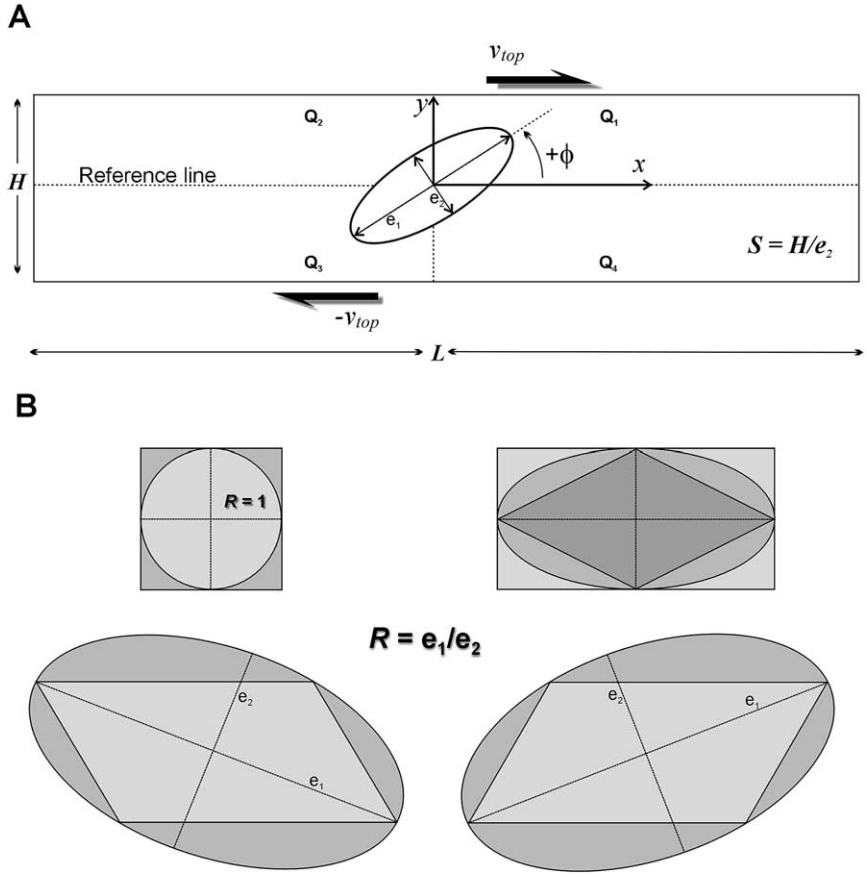

Fig. 1. (A) Representation of the computational domain with an elliptical inclusion. H and L are the height and length of the domain; e_1 and e_2 are the principal axes of the elliptical inclusion; ϕ is the angle between e_1 and X, and is positive anticlockwise; Q_n are quadrants from 1 to 4. The shear direction is parallel to the X-axis and the sense of shear is top to right in all the models. (B) Shapes used in this study and respective aspect ratios (R). Adapted from Marques et al. (2005).

rotation behaviour of rigid elliptical inclusions, and lead to the development of stable shape preferred orientations (SPO) in simple shear.

Ghosh and Ramberg (1976), Arbaret et al. (2001) and Schmid (in press) showed, using analogue experiments and analytical solutions, that the behaviour of rigid inclusions of different shapes embedded in a Newtonian matrix undergoing simple shear is not significantly different from that predicted for an enveloping ellipse by Jeffery's analytical solution. It thus appears that shape does not matter in wide channels; what matters is the inclusion's aspect ratio. In the present paper, we show that the shape matters in confined flow. Mancktelow et al. (2002), Ceriani et al. (2003) and Marques and Bose (2004) investigated the effects of shape on rotation behaviour, but only for the slipping mode, which is not the case of the present paper.

In view of the above state of the art and following the work initiated by Marques and Cobbold (1995), we carried out a numerical study with the following objectives: (i) to investigate the effects of confinement on rigid inclusion rotation under viscous simple shear; and (ii) to analyse the effects of inclusion's aspect ratio, shape and initial orientation on rotation. The numerical models provide a wealth of physical information that was lacking in the experimental work of Marques and Cobbold (1995) and Marques and Coelho (2001). We are aware of the shortcomings of a 2D study, especially if we accept that the rigid inclusions rotate in the manner proposed by Jeffery (1922). However, we are now studying a quite different situation, which is rotation under confinement. Therefore, we do not yet know how the rigid inclusions rotate in 3D, under confinement, to compare with Jeffery's results. Besides, the only experimental data in conditions of confined flow available for comparison are also 2D.

2. Model formulation and boundary conditions

Icompressible viscous fluid rheology is widely accepted as a simple but effective approximation to the behaviour of rocks undergoing ductile deformation. The mathematical model used in the present work is based on the 2D steady-state incompressible Navier–Stokes equations (e.g. Granger, 1994)

$$\rho\left(\frac{\partial \mathbf{u}}{\partial \mathbf{t}} + \mathbf{u}\cdot\nabla\mathbf{u}\right) = -\nabla p + \eta\nabla^2\mathbf{u} + \mathbf{F} \quad (1)$$

$$\nabla\cdot\mathbf{u} = 0 \quad (2)$$

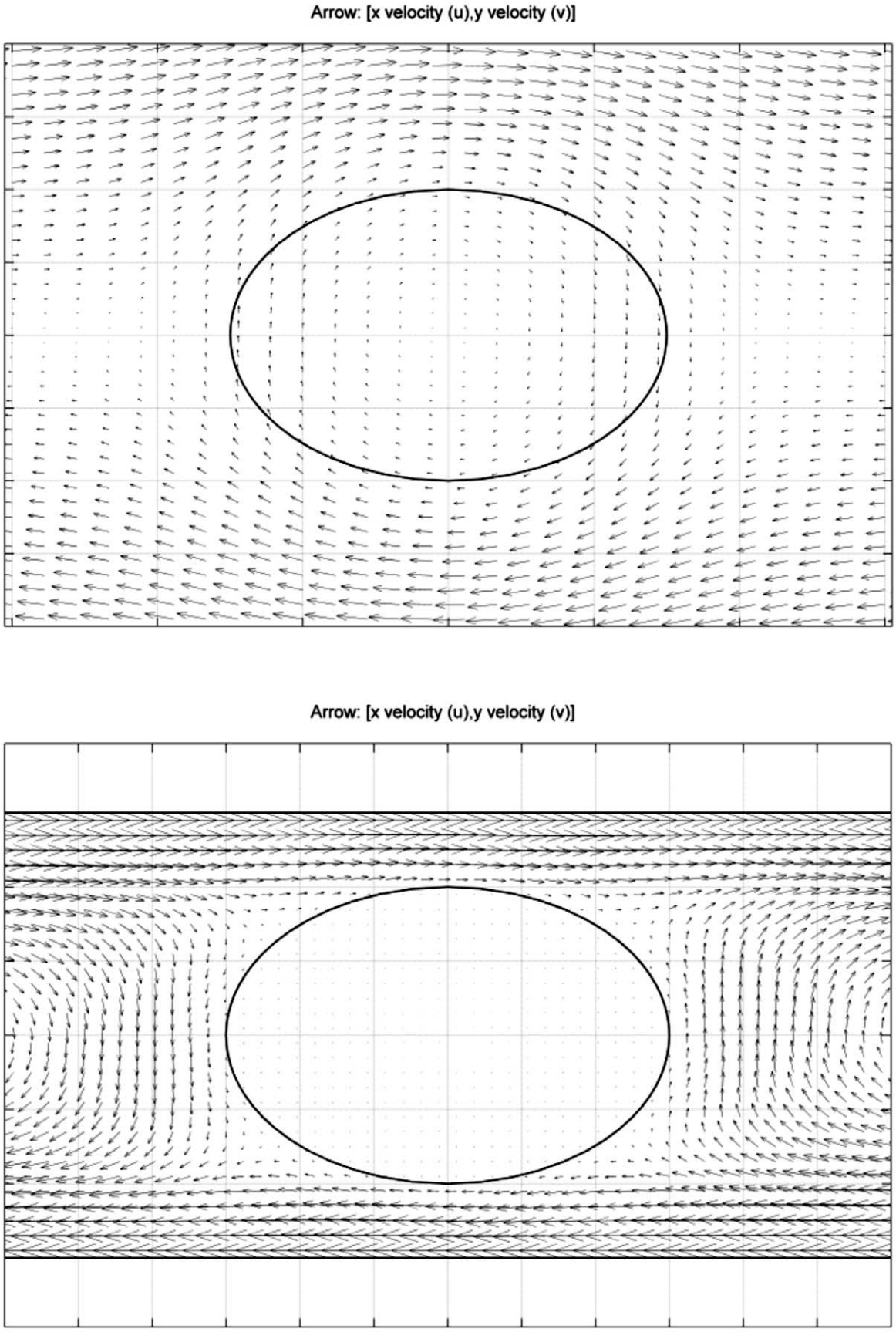

Fig. 2. Velocity vector fields close to the inclusion for $S = 10.0$ (A) and 1.5 (B). Note that in (A), the velocities in the matrix all work for the synthetic rotation of the inclusion and that in (B) a good deal of the matrix flow induces antithetic rotation of the inclusion. Sense of shear is top to right.

where **u** is the velocity vector, p the pressure, ρ the density, η the dynamic viscosity and **F** the external body force (ρ and η are constants and **F** will be assumed negligible in this model).

The boundary conditions needed to complete the mathematical formulation and define a simple shear flow were (i) velocity set to values $\pm V_{top}$ at $Y = \pm H/2$ (Fig. 1a), and (ii) velocity set to vary linearly between the top and bottom velocities (with zero-mean) at the left and right end boundaries (straight-out condition). The above equations were solved in the 2D rectangular domain illustrated in Fig. 1a, which was filled with an incompressible linear viscous fluid with matrix viscosity (μ) set to 1. High-viscosity fluid-modelled inclusions ($\mu = 1.0e+6$) were positioned at the centre of the domain (x, $y = 0$). The boundaries between inclusion and matrix were set to neutral (perfectly bonded), which means that the rigid inclusion follows the flow passively. Therefore, the rotation of the rigid inclusion is the result of the velocities applied at the top and bottom boundaries. The width of the computational domain was chosen according to the desired confinement ($S = H/e_2$). The length (L) was set to about 30 times the greatest inclusion axis (e_1). The flow equations, with the boundary conditions specified, were solved in the primitive variables $\mathbf{u} \equiv (u,v)$ (u and v being the X and Y components of velocity, respectively) and P over a finite element mesh, using the algorithm for stationary incompressible Navier–Stokes flows using the finite-element program FEMLAB (2002). Pressure, velocity and vorticity were computed, step-by-step, for different angles of inclusion orientation. The mesh was refined for the cases of $S = 1.2$ and 1.5. Further details of the computational method and numerical procedures can be found in Gresho and Sani (2000).

The inclusion shapes studied were ellipses, rectangles, lozenges and skewed rectangles (Fig. 1b), with the aspect ratios ($R = e_1/e_2$) equal to 1, 1.5, 3 and 6, to simulate the most common shapes found in natural shear zones. To determine the rectangle R, we found the ratio between the long and short sides (inscribed ellipse as in Ghosh and Ramberg (1976)). For skewed rectangles, we used the aspect ratio of the circumscribed ellipse where e_1 is coincident with the longest diagonal of the skewed rectangle. In this case, the longest ellipse axis is inclined relative to X when the long sides of the inclusion are parallel to X. The angle between the instantaneous direction of e_1 and the shear direction (X) is the inclusion orientation (ϕ), which is positive anticlockwise. There are two orientations for which the inclusion rotation rate is zero: the stable (ϕ_{se}) and unstable (ϕ_{ue}) equilibrium orientations.

3. Numerical results

3.1. Velocity

A detailed description of the velocities around the inclusions might be very interesting but is kept short due to space constraints. We have restricted description to the most relevant situations for the understanding of inclusion rotation. The velocity vector fields for the ellipse in wide and narrow channels are represented in Fig. 2.

When the channel is wide ($S > 10$), the X-component of the velocity field is always positive in the matrix in the upper half of the model (Fig. 2a) and negative in the lower half, in agreement with the applied far field velocity and matrix vorticity. On the other hand, when the flow is confined, e.g. $S = 1.5$ (Fig. 2b), there are regions around the inclusion where the X-component of the velocity field is negative in the upper half and positive in the lower half, i.e. where there is back-flow. When $S > 10$, the Y-component of the velocity field close to the inclusion is always positive in quadrants 2 and 3 (Q_2 and Q_3), and negative in Q_1 and Q_4 (Fig. 2a). When S is small, the Y-component of the velocity field close to the inclusion is negative in much of Q_2 and Q_3, and positive in much of Q_1 and Q_4 (Fig. 2b).

3.2. Pressure

Colour maps were developed to evaluate pressure in the matrix (Fig. 3). The feature common to all shapes is the pressure distribution by quadrants in the matrix, especially at $\phi = 0°$. The higher pressure quadrants in the matrix are in the contraction quadrants of simple shear, and the lower pressure quadrants are in the expansion quadrants. Pressure in the matrix changes configuration with confinement and inclusion rotation. The pressure magnitude increases significantly with confinement, as can be inferred from the examples shown in Fig. 3.

3.3. Vorticity

Once the inclusion is quasi-rigid, its angular velocity can be estimated using the vorticity computed at an arbitrary point inside the inclusion, here defined as $((\partial \mathbf{v}_y/\partial \mathbf{x}) - (\partial \mathbf{v}_x/\partial \mathbf{y}))$, with an advantage that one can compare the vorticities of inclusion and matrix. When the vorticity is zero, the inclusion is in an equilibrium orientation, either stable (ϕ_{se}) or unstable (ϕ_{ue}); when it is negative, the inclusion is rotating clockwise (synthetic in our models); when it is positive, the inclusion is rotating anticlockwise (antithetic in our models). The stability character of each equilibrium solution can be found through the numerical derivative of the rotation rate over the orientation ($\partial\dot{\phi}/\partial\phi$): if it is positive, the equilibrium is unstable, and if it is negative the equilibrium is stable.

The numerical results for inclusion rotation in the confined flow are summarised in Table 1 and represented as graphs in Fig. 4. Comparison between the rotation behaviour of all inclusion shapes shows that:

(1) Inclusion rotation behaves in two distinct ways when S allows a full revolution: (i) near-sinusoidal with more than one wavelength within 180° of inclusion rotation,

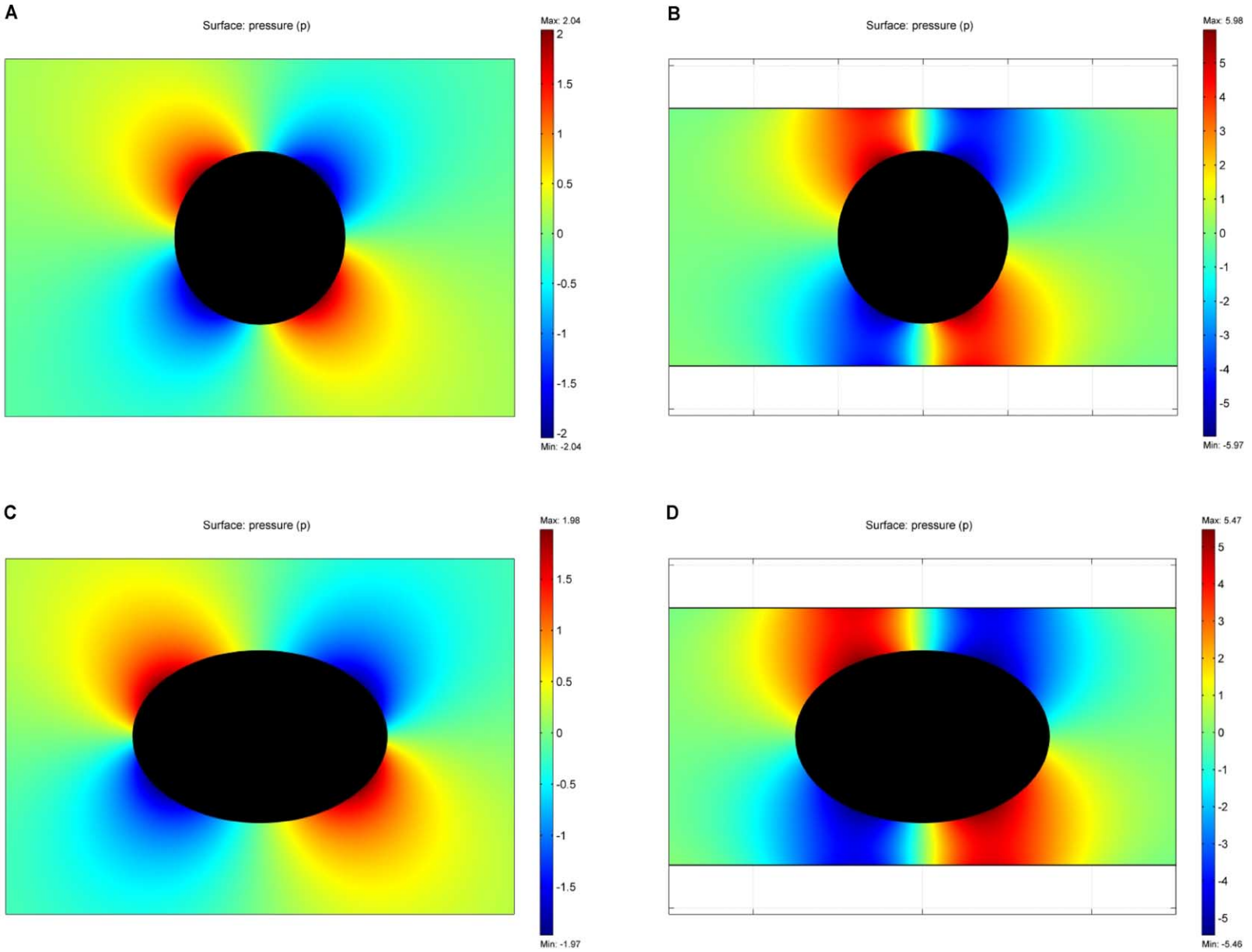

Fig. 3. Colour maps to illustrate confinement effects on pressure (in Pa) for the circle at $S = 10.0$ (A) and 1.5 (B), and for the ellipse at $S = 10.0$ (C) and 1.5 (D). Pressure inside the rigid inclusions is not shown (black fill). Sense of shear is top to right.

Table 1
Summary of the numerical results on inclusion rotation, regarding stable (ϕ_{se}) and unstable (ϕ_{ue}) equilibrium orientations

			Ellipse	Rectangle	Rectangle		Lozenge
					Skew right	Skew left	
$R=1.0$	$S=1.2$	ϕ_{se}	**NE**	(*1)			
		ϕ_{ue}	**NE**	(*1)			
	$S=1.5$	ϕ_{se}	**NE**	**NE**			
		ϕ_{ue}	**NE**	**NE**			
$R=1.5$	$S=1.2$	ϕ_{se}	(*2) 24	(*3)	(*4) 0	(*6) 2	(*8) 26
		ϕ_{ue}	(*2) −24	(*3)	(*5) −2	(*7) 0	(*8) 26
	$S=1.5$	ϕ_{se}	(*9) 8	(*10)	(*11) 0	(*13) 7	**11**
		ϕ_{ue}	(*9) −8	(*10)	(*12) −7	(*14) 0	**−11**
	$S=2.0$	ϕ_{se}	**NE**	**NE**	(*15) −1	(*17) 14	**NE**
		ϕ_{ue}	**NE**	**NE**	(*16) −14	(*18) 1	**NE**
	$S=3.0$	ϕ_{se}	**NE**	**NE**	**NE**	**NE**	**NE**
		ϕ_{ue}	**NE**	**NE**	**NE**	**NE**	**NE**
$R=3.0$	$S=1.2$	ϕ_{se}	(*1) 12	(*19) 0.5	(*20) 0	(*22) 1.5	(*24) 18
		ϕ_{ue}	(*1) −12	(*19) −0.5	(*21) −1.5	(*23) 0	(*24) −18
	$S=1.5$	ϕ_{se}	(*24) 14	(*25) 1.5	(*26) 0	(*28) 5	(*30) 18
		ϕ_{ue}	(*24) −14	(*25) −1,5	(*27) −5	(*29) 0	(*30) 18
	$S=4.0$	ϕ_{se}	**5**	**NE**	(*31) 2	(*33) 22	**9**
		ϕ_{ue}	**−4**	**NE**	(*32) −22	(*34) −2	**−9**
	$S=5.0$	ϕ_{se}	**NE**	**NE**	(*35) 1	(*37) 20	**4**
		ϕ_{ue}	**NE**	**NE**	(*36) −20	(*38) −1	**−4**
	$S=8.0$	ϕ_{se}	**NE**	**NE**	**−2**	**14**	**NE**
		ϕ_{ue}	**NE**	**NE**	**−14**	**2**	**NE**
	$S=10.0$	ϕ_{se}	**NE**	**NE**	**NE**	**NE**	**NE**
		ϕ_{ue}	**NE**	**NE**	**NE**	**NE**	**NE**
$R=6.0$	$S=1.2$	ϕ_{se}	(*39) 6	(*40) 0.5	(*41) 0	(*43) 1	(*45) 9
		ϕ_{ue}	(*39) −6	(*40) −0.5	(*42) −1	(*44) 0	(*45) −9
	$S=1.5$	ϕ_{se}	(*46) 7	(*47) 0.5	(*48) 0	(*50) 2.5	(*52) 9
		ϕ_{ue}	(*46) 7	(*47) 0.5	(*49) 2.5	(*51) 0	(*52) −9
	$S=10.0$	ϕ_{se}	**5**	**NE**	(*53) 3	(*55) 13	**6**
		ϕ_{ue}	**−5**	**NE**	(*54) −13	(*56) −3	**−6**
	$_S=12.0$	ϕ_{se}	**NE**	**NE**	**3**	**12**	**3**
		ϕ_{ue}	**NE**	**NE**	**−12**	**−3**	**−3**
	$S=20.0$	ϕ_{se}	**NE**	**NE**	**0**	**10**	**NE**
		ϕ_{ue}	**NE**	**NE**	**−10**	**0**	**NE**
	$S=24.0$	ϕ_{se}	**NE**	**NE**	**NE**	**NE**	**NE**
		ϕ_{ue}	**NE**	**NE**	**NE**	**NE**	**NE**

Full inclusion rotation is possible for bold items. NE, non-existent stable or unstable equilibrium orientations in a full rotation. *n, full inclusion rotation is not possible because inclusion touches the shear zone walls after some rotation from $\phi=0°$: *1–±13°; *2–±35°; *3–±8°; *4–−4°; *5–−6°; *6–6°; *7–−4°; *8–±53°; *9—±80°; *10–±22°; *11–10°; *12–−16°; *13–16°; *14–−10°; *15–23°; *16–−37°; *17–37°; *18–−23°; *19–±4°; *20–2°; *21–−3°; *22–3°; *23–−2°; *24–±23°; *25–±10°; *26–5°; *27–−9°; *28–9°; *29–−5°; *30–±30°; *31–33°; *32–−51°; *33–51°; *34–−33°; *35–46°; *36–−65°; *37–65°; *38–−46°; *39–±6.5°; *40–±2°; *41–1°; *42–−2°; *43–2°; *44–−1°; *45–±12°; *46–±11°; *47–±5°; *48–2°; *49–−5°; *50–5°; *51–−2°; *52–±15°; *53–52°; *54–−62°; *55–62°; *56–−52°.

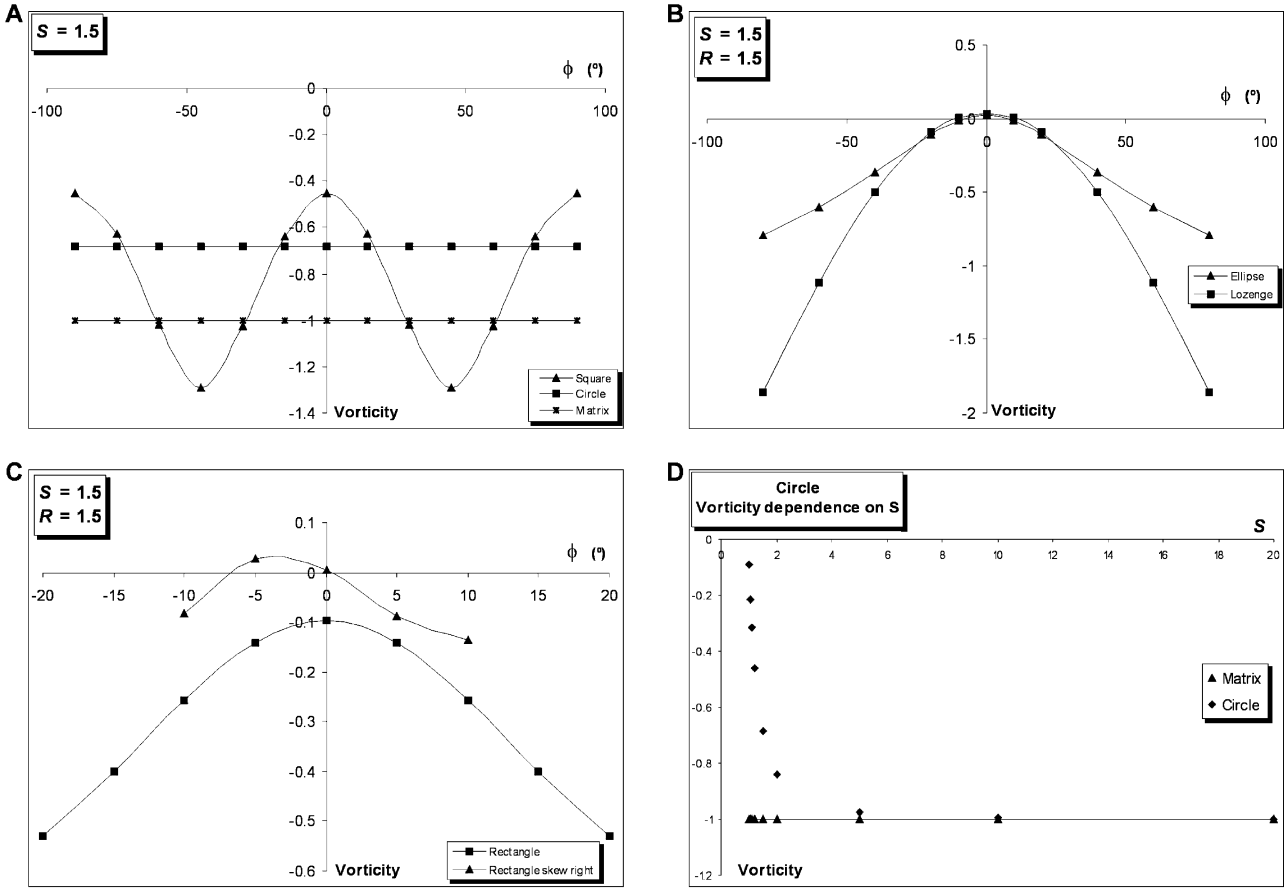

Fig. 4. Graphs to illustrate evolution of vorticity with inclusion orientation for $S=1.5$. Note that $S=1.5$ does not allow a full revolution of the rectangle and skewed rectangle. (D) Graph to illustrate the dependence of circle rotation on S.

which is the case of the square (Fig. 4a), and (ii) near-sinusoidal or just oscillating with half-wavelength within 180° of inclusion rotation for all other shapes.

(2) The rotation behaviour of the circle in the confined flow is significantly different from that of the square, despite the identical R. The circle vorticity is constant (Fig. 4a) but depends on S (Fig. 4d), as also shown by Biermeier et al. (2001), and only approximates the far field matrix vorticity (-1) for S values greater than 5. The circle's vorticity curve is asymptotic relative to X and Y, approaching -1 with increasing S and approaching 0 with decreasing S. In contrast to the circle, the square's vorticity is oscillating (Fig. 4a), depending on the orientation of the square's sides relative to X. When there is no ϕ_{se}, the rotation of inclusions with $R>1$ is also oscillating.

(3) There are two orientations for which the inclusion rotation rate can be zero in inclusions with $R>1$, ϕ_{se} and ϕ_{ue}. Note, however, that R values for which there is a ϕ_{se} change significantly with shape. For instance, at $S=5.0$ and $R=3.0$, only the skewed rectangles and the lozenge have ϕ_{se}, and if S increases to 8 only the skewed rectangles have ϕ_{se}.

(4) The values of ϕ_{se} and ϕ_{ue} given in Table 1 for the skewed rectangles are valid only for the chosen skew angle.

(5) Synthetic and antithetic rotations are limited when there is ϕ_{se}, independent of the amount of shear deformation thereafter.

(6) The angular values of ϕ_{se} and ϕ_{ue} depend on S, and when the confinement is effective, shape and R also play an important role. However, there seems to be no common rule for the computed ϕ_{se} and ϕ_{ue} variations.

(7) The shapes of the inclusion vorticity curves are similar for all shapes with $R>1$ when there is a ϕ_{se}, but the values change significantly with S, shape and R.

4. Discussion

One major result of our numerical model is that all studied shapes with $6\geq R>1$ may display ϕ_{se} and ϕ_{ue}, depending on S, with the exception of a rectangle with $R=1.5$.

In our model, pressure and viscous effects on the inclusion perimeter result from the computed velocity and pressure fields. The issue is their relative importance in the

process. As shown in Section 3.1, in non-confined flow, the X-component of the velocity field is always positive in the upper half of the model and negative in the lower half, which indicates an overall clockwise rotation (negative vorticity of the flow) that drives the inclusion's synthetic rotation. It means that the inclusion is following the viscous flow passively. This contrasts with the confined case, in which there are regions around the inclusion where the X-component of the velocity field is negative in the matrix in the upper half of the model and positive in the lower half, i.e. where there is back flow (Fig. 2). Therefore, one part of the flowing matrix is driving synthetic rotation and another part is forcing antithetic rotation. The Y-component of the velocity field plays a similar role to that played by the X-component. This means that the inclusion is resisting flow and rotation according to matrix far field vorticity. On the other hand, pressure gradients around the inclusion greatly increase with confinement. In quadrants 1 and 3, the pressure is negative, and in quadrants 2 and 4 the pressure is positive; these pressure gradients drive antithetic inclusion rotation because the inclusion rotates simultaneously away from pressure highs and towards pressure lows. Therefore, matrix flow and pressure gradients add effects to make the inclusions rotate antithetically in the confined flow.

Concerning inclusion rotation, this study shows that:

1. The rigid circle and the square rotate differently, which means that shape matters in the confined, non-slipping mode for inclusions with $R=1$. In the case of the circle, normal stresses induced by the flowing matrix cannot play a direct role in rotation because they cannot generate torques. Therefore, shear stresses alone govern rotation (whatever their magnitude). Although the rotation rate of the circle approaches zero with confinement (Fig. 4d), it is never zero. Therefore, our model cannot explain the hypothesis of Bell and Johnson (1989) that spherical inclusions like garnet do not rotate when embedded in a matrix undergoing simple shear flow (see also Jung et al., 1999; Bell and Kim, 2004; Bell et al., 2004).
2. Inclusion rotation depends strongly on S. With confinement, the vorticity, velocity and pressure fields change in the matrix around the inclusion, which affects the inclusion rotation.
3. ϕ_{se} and ϕ_{ue} depend strongly on the shape for identical R when the confinement is effective. The contrasting geometries of the inclusions, and in particular the disposition of the geometric elements of each shape relative to the far field flow, control the distributions and magnitudes of normal and shear stresses along the inclusion surface, and therefore determine inclusion rotation behaviour. Good examples are the ellipse and the rectangle at $\phi=0°$. The ellipse shows a smooth rounded perimeter that gradually changes orientation relative to the matrix flow, in great contrast to the angular character of the rectangle perimeter, with short sides normal to and long sides parallel to the far field flow. Again, shape matters in this mode for identical R.
4. The $\phi=0°$ of the skewed rectangles was taken in this study as the orientation in which the long sides are parallel to X. This is inconsistent with the definition given above, but it seems reasonable when we compare with the rectangle at $\phi=0°$. If we take the definition strictly, the $\phi=0°$ of the skewed rectangles should be when the enveloping ellipse is at $\phi=0°$. Therefore, the curve in the graph of Fig. 4c should be translated by 19° parallel to X, which is the dip of the enveloping ellipse when the long sides of the skewed rectangle are parallel to X.

5. Geological significance

Where can we find confinement in nature? It can be found in layered rocks like sedimentary, metamorphic or magmatic rocks. Layers of contrasting mineral composition usually show different rheological behaviour, indicating that flow can be markedly heterogeneous. The different rheological behaviour between adjacent layers can concentrate shear deformation in narrow ductile zones of softer rock bounded by harder rock, and lead to confined flow. The photograph of a natural ductile shear zone in Fig. 5 illustrates confinement. Again, different rheological behaviour between layers of contrasting mineralogy leads to shear concentration: the softer mylonites inside the ductile shear zone are mostly composed of calcite ($\pm$silicates), bounded by harder mafic granulite rich in garnet, pyroxene and plagioclase. An elliptical 'rigid inclusion' of mafic granulite tilted opposite to the shear sense, which is top to right, is present within the shear zone. Our interpretation is that this is a stable equilibrium orientation resulting from the confined flow. Information on the geological setting of the rocks illustrated in Fig. 5 can be found in Marques et al. (1996).

6. Conclusions

To summarise, we conclude that:

(1) Inclusion rotation is strongly influenced by S and, when confinement is effective, aspect ratio and shape also play an important role.
(2) Inclusions with the aspect ratio equal to one still rotate synthetically when confined, but at a rate that depends upon S, shape (circle or square) and orientation, which is not the case in the non-confined mode.
(3) Ellipses, rectangles, lozenges and skewed rectangles may rotate antithetically when starting with $\phi=0°$, depending on confinement. Back rotation is limited because the inclusions reach a stable equilibrium orientation (ϕ_{se}).

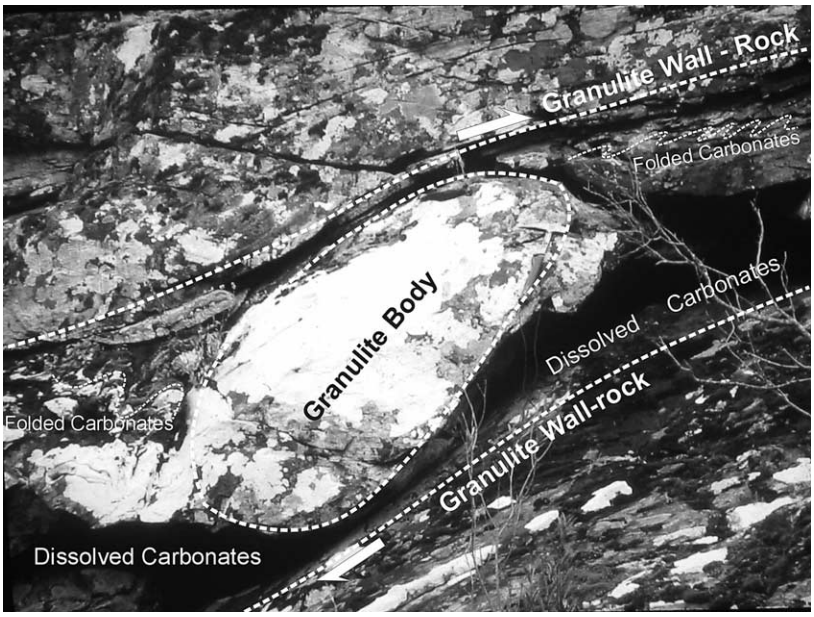

Fig. 5. Photograph of natural occurrence from the Bragança Massif, NE Portugal, to illustrate the possible confinement. Softer mylonites inside a ductile shear zone, mostly composed of calcite (±silicates), are bounded by harder mafic granulites rich in garnet, pyroxene and plagioclase, which acted as the shear zone walls. The elliptical 'rigid inclusion' of mafic granulite observed within the shear zone is tilted opposite to the shear sense and is interpreted as a stable equilibrium orientation resulting from the confined flow. Hammer for scale at top right of the granulite inclusion. Adapted from Marques and Cobbold (1995).

(4) There is also an unstable equilibrium orientation (ϕ_{ue}), which defines an antithetic rotation field with ϕ_{se}, and both ϕ_{se} and ϕ_{ue} depend on S, and inclusion R and shape.
(5) Matrix re-flux and pressure gradients add effects to make the inclusions rotate antithetically in confined flow.

Acknowledgements

This is a contribution to research project TEAMINT (POCTI/CTA/48137/2002). Constructive reviews by J. Ježek and L. Arbaret, and editorial work by J. Hippertt are gratefully acknowledged. We thank Paul Covill for having corrected the English. We thank IBM Portugal for computational support, in particular Paulo Antunes and Hugo Figueiredo.

References

Arbaret, L., Mancktelow, N., Burg, J.-P., 2001. Effect of shape and orientation on rigid particle orientation and matrix deformation in simple shear flow. Journal of Structural Geology 23, 113–125.
Bell, T.H., Johnson, S.E., 1989. Porphyroblast inclusion trails: the key to orogenesis. Journal of Metamorphic Geology 7, 279–310.
Bell, T.H., Kim, H.S., 2004. Preservation of Acadian deformation and metamorphism through intense Alleghanian shearing. Journal of Structural Geology 26, 1591–1613.
Bell, T.H., Ham, A.P., Kim, H.S., 2004. Partitioning of deformation along an orogen and its effects on porphyroblast growth during orogenesis. Journal of Structural Geology 26, 825–845.
Biermeier, C., Stüwe, K., Barr, T.D., 2001. The rotation rate of cylindrical objects during simple shear. Journal of Structural Geology 23, 765–776.
Ceriani, S., Mancktelow, N.S., Pennacchioni, G., 2003. Analogue modelling of the influence of shape and particle/matrix interface lubrication on the rotational behaviour of rigid particles in simple shear. Journal of Structural Geology 25, 2005–2021.
FEMLAB 2.3 Reference Manual, 2002. Comsol AB, Tegnérgatan 23, SE-111 40 Stockholm, Sweden.
Fernandez, A., Feybesse, J.L., Mezure, J.F., 1983. Theoretical and experimental study of fabrics developed by different shaped markers in two-dimensional simple shear. Bulletin Societé Géologique France 25, 319–326.
Ghosh, S.K., Ramberg, H., 1976. Reorientation of inclusions by combination of pure and simple shear. Tectonophysics 34, 1–70.
Granger, R.A., 1994. Fluid Mechanics. Dover Classics of Science and Mathematics.
Gresho, P.M., Sani, R.L., 2000. Incompressible Flow and the Finite Element Method, vols. 1 and 2. Wiley, New York.
Hudleston, P.J., Lan, L., 1994. Rheological controls on the shapes of single-layer folds. Journal of Structural Geology 16, 1007–1021.
Ildefonse, B., Mancktelow, N.S., 1993. Deformation around rigid particles: the influence of slip at the particle/matrix interface. Tectonophysics 221, 345–359.
Ildefonse, B., Launeau, P., Bouchez, J.-L., Fernandez, A., 1992a. Effect of mechanical interactions on the development of shape preferred orientations: a two-dimensional experimental approach. Journal of Structural Geology 14, 73–83.
Ildefonse, B., Sokoutis, D., Mancktelow, N.S., 1992b. Mechanical interactions between rigid particles in a deforming ductile matrix. Analogue experiments in simple shear flow. Journal of Structural Geology 14, 1253–1266.
Jeffery, G.B., 1922. The motion of ellipsoidal particles immersed in a viscous fluid. Proceedings of the Royal Society of London, Series A 102, 161–179.

Ježek, J., Melka, R., Schulmann, K., Venera, Z., 1994. The behaviour of rigid triaxial particles in viscous flows—modelling of fabric evolution in a multiparticle system. Tectonophysics 229, 165–180.

Ježek, J., Schulmann, K., Segeth, K., 1996. Fabric evolution of rigid inclusions during mixed coaxial and simple shear flows. Tectonophysics 257, 203–221.

Jung, W.S., Ree, J.H., Park, Y., 1999. Non-rotation of garnet porphyroblasts and 3-D inclusion trail data: an example from the Imjingang belt, South Korea. Tectonophysics 307, 381–395.

Mancktelow, N.S., Arbaret, L., Pennacchioni, G., 2002. Experimental observations on the effect of interface slip on rotation and stabilisation of rigid particles in simple shear and a comparison with natural mylonites. Journal of Structural Geology 24, 567–585.

Marques, F.O., Bose, S., 2004. Influence of a permanent low-friction boundary on rotation and flow in rigid-inclusion/viscous-matrix systems from an analogue perspective. Tectonophysics 382, 229–245.

Marques, F.G., Cobbold, P.R., 1995. Development of highly non-cylindrical folds around rigid ellipsoidal inclusions in bulk simple shear: natural examples and experimental modelling. Journal of Structural Geology 17, 589–602.

Marques, F.O., Coelho, S., 2001. Rotation of rigid elliptical cylinders in viscous simple shear flow: analogue experiments. Journal of Structural Geology 23, 609–617.

Marques, F.O., Coelho, S., 2003. 2-D shape preferred orientations of rigid particles in transtensional viscous flow. Journal of Structural Geology 25, 841–854.

Marques, F.O., Ribeiro, A., Munhá, J.M., 1996. Geodynamic evolution of the Continental Allochthonous Terrane (CAT) of the Bragança Nappe Complex, NE Portugal. Tectonics 15, 747–762.

Marques, F.O., Taborda, R., Bose, S., Antunes, J., 2005. Effects of confinement on matrix flow around a rigid inclusion in viscous simple shear: insights from analogue and numerical modelling. Journal of Structural Geology 27, 379–396.

Passchier, C.W., 1987. Stable positions of rigid objects in non-coaxial flow—a study in vorticity analysis. Journal of Structural Geology 9, 679–690.

Passchier, C.W., ten Brink, C.E., Bons, P.D., Sokoutis, D., 1993. δ objects as a gauge for stress sensitivity of strain rate in mylonites. Earth and Planetary Science Letters 120, 239–245.

Pennacchioni, G., Fasolo, L., Cecchi, M.M., Salasnich, L., 2000. Finite-element modelling of simple shear flow in Newtonian and non-Newtonian fluids around a circular rigid particle. Journal of Structural Geology 22, 683–692.

Pennacchioni, G., di Toro, G., Mancktelow, N., 2001. Strain-insensitive preferred orientation of porphyroclasts in Mont Mary mylonites. Journal of Structural Geology 23, 1281–1298.

Samanta, S.K., Mandal, N., Chakraborty, C., 2003. Flow patterns around rigid inclusions in a multiple inclusion system undergoing bulk simple shear deformation. Journal of Structural Geology 25, 209–221.

Schmalholz, S.M., Podladchikov, Y.Y., 2001. Strain and competence contrast estimation from fold shape. Tectonophysics 340, 195–213.

Schmid, D.W., 2005. Rigid polygons in shear. In: Bruhn, D., Burlini, L. (Eds), High Strain Zones: Structure and Physical Properties. Geological Society of London Special Publications 245, 421–431.

Schmid, D.W., Podladchikov, Y.Y., 2004. Are isolated stable rigid clasts in shear zones equivalent to voids? Tectonophysics 384, 233–242.

Taborda, R., Antunes, J., Marques, F.O., 2004. 2-D rotation behavior of a rigid ellipse in confined viscous simple shear: numerical experiments using FEM. Tectonophysics 379, 127–137.